Durham University

Durham Research Online

Deposited in DRO:

31 October 2016

Version of attached file:

Accepted Version

Peer-review status of attached file:

Peer-reviewed

Citation for published item:

Nowakowski, P. J. and Woods, D. A. and Verlet, J. R. R. (2016) 'Charge transfer to solvent dynamics at the ambient water/air interface.', Journal of physical chemistry letters., 7 (20). pp. 4079-4085.

Further information on publisher's website:

https://doi.org/10.1021/acs.jpclett.6b01985

Publisher's copyright statement:

This document is the Accepted Manuscript version of a Published Work that appeared in final form in Journal of physical chemistry letters, copyright © American Chemical Society after peer review and technical editing by the publisher. To access the final edited and published work see https://doi.org/10.1021/acs.jpclett.6b01985.

Additional information:

Use policy

The full-text may be used and/or reproduced, and given to third parties in any format or medium, without prior permission or charge, for personal research or study, educational, or not-for-profit purposes provided that:

- a full bibliographic reference is made to the original source
- a link is made to the metadata record in DRO
- the full-text is not changed in any way

The full-text must not be sold in any format or medium without the formal permission of the copyright holders.

Please consult the full DRO policy for further details.

Durham University Library, Stockton Road, Durham DH1 3LY, United Kingdom
Tel : +44 (0)191 334 3042 | Fax : +44 (0)191 334 2971
https://dro.dur.ac.uk

Charge Transfer to Solvent Dynamics at the Ambient Water/Air Interface

*Paweł J. Nowakowski, David A. Woods and Jan R. R. Verlet**

Department of Chemistry, University of Durham, Durham DH1 3LE, U.K.

Abstract

Electron transfer reactions at the ambient aqueous interfaces represent one of the most fundamental and ubiquitous chemical reactions. Here, the dynamics of the charge transfer to solvent (CTTS) reaction from iodide was probed at the ambient water/air interface by phase-sensitive transient second harmonic generation. Using the three allowed polarisation combinations, distinctive dynamics assigned to the CTTS state evolution and to the subsequent solvating electron-iodine contact pair have been resolved. The CTTS state is asymmetrically solvated in the plane of the surface, while the subsequent electron solvation dynamics are very similar to those observed in the bulk, although slightly faster. Between 3 and 30 ps, a small phase shift distinguishes an electron bound in a contact pair with iodine and a free hydrated electron at the water/air interface. Our results suggest that the hydrated electron is fully solvated in a region of reduced water density at the interface.

TOC graphic:

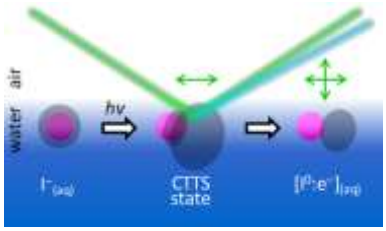

*E-mail: j.r.r.verlet@durham.ac.uk

Electron transfer reactions in aqueous solution represent one of the most fundamental chemical processes with broad importance in fields such as chemical biology, electrochemistry, radiation chemistry and atmospheric chemistry.[1] Of these reactions, the charge transfer to solvent (CTTS) reaction from a solute anion has been a prototype: it provides a unique opportunity to probe the initial dynamics of the surrounding water molecules as they reorient on an ultrafast timescale to solvate the new charge distribution, eventually forming a hydrated electron, $e^-_{(aq)}$. A particularly useful means of initiating CTTS reactions is photoexcitation to CTTS absorption bands of certain aqueous anions. The most studied of these has been the CTTS of iodide[2–13] and a schematic of the solvation dynamics are shown in Figure 1. However, these studies have focussed on the bulk dynamics, while arguably, electron transfer reactions are of most interest at interfaces, be it on an aerosol particle, on an interstellar dust-grain, or at a water/biomolecule interface. In an attempt to probe interfacial CTTS dynamics of iodide, time-resolved photoelectron spectroscopy coupled with the liquid microject technique has recently been used.[6,9–13] Results from such experiments showed that the observable dynamics are very similar to those seen in the bulk. However, questions remain about that method's surface sensitivity, which is governed by the photoelectron's inelastic mean free path in the microjet, and about the nature of the surface at the vacuum/water interface in a liquid microjet. The only measurement of CTTS dynamics at an ambient water/air interface was performed using time-resolved second harmonic generation (SHG) spectroscopy,[14] which is surface sensitive by virtue of the 2nd order non-linear nature of the SHG interaction, with the surface sensitivity defined by the depth over which inversion symmetry is broken. This experiment also showed dynamics similar to those observed in the bulk, suggesting very little influence of the surface on the observable dynamics, but suffered from complications arising from the nonlinear nature of the experiment. Here, we overcome these limitations and revisit the dynamics of the CTTS

reaction from iodide at the ambient water/air interface using a phase-sensitive time-resolved SHG experiment and show, using different symmetry-allowed polarisation combinations, that distinctive surface solvation dynamics can be seen at the interface.

Experimentally, a 250 nm femtosecond pump pulse was used to initiate the CTTS process in a 2 M aqueous solution of NaI. As iodide partitions to both the bulk and the surface of water,[15] the CTTS dynamics will be initiated at the water/air surface and in the bulk. To probe only the water/air interface, we employ phase-sensitive SHG. Phase-sensitive SHG has been used both non-spectroscopically[16–18] and spectroscopically[19,20] and recently, a number of groups have combined this into time-resolved and phase-sensitive SHG,[21–23] primarily for use at semiconductor interfaces. We have developed a variant of these techniques that is not spectroscopic but benefits from a lock-in measurement and excellent phase stability, which is crucial to the current measurements.[24] The time-resolution of the experiment is approximately 100 fs.

Figure 2 shows contour plots of the amplitude of the phase- and time-resolved SHG for the three symmetry-allowed polarisation combinations at two different fundamental wavelengths (1320 nm and 800 nm). The allowed polarisation combinations are PP, PS, and Smix, where the first letter denotes the polarisation of the SHG light and the second the polarisation of the fundamental light; mix refers to a mixture between S and P polarisations. The data have been fitted globally (see supporting materials) to recover the amplitude and the absolute phase of the time-resolved SHG signal. The amplitude is shown as insets on the left of each phase- and time-resolved SHG plot, while the absolute phase is shown as a black dashed line (the red dashed line shows a phase shift of $\pm\pi$). The phase is related to the real and imaginary parts the nonlinear second-order susceptibility, $\chi^{(2)}$. When a transition is exactly resonant with either ω or 2ω (where ω is the angular frequency of the light), the contribution to $\chi^{(2)}$ from that transition will be purely imaginary, while the real part of $\chi^{(2)}$

changes sign either side of the transition. In contrast to the linear susceptibility, it is possible for both ω or 2ω to be resonant in SHG, in which case the main contribution to $\chi^{(2)}$ will be real while the imaginary part will change sign across the transition. The overall $\chi^{(2)}$ observed is the sum of the contributions of all the transitions. An observed temporal phase shift can arise for two reasons: either a specific transition is spectrally shifting as time evolves, or the ratio of intensities between multiple transitions with different phases is changing. For the evolving CTTS state and subsequent hydrated electron, a large number of transitions may contribute and a quantitative assignment of the phase is beyond the scope of this work. Instead, phase shifts provide an additional qualitative measure of dynamics and these are considered here along with the amplitude dynamics.

The amplitudes shown in Figure 2 are not directly comparable with each other; however, the relative intensities of the different polarisation combinations and probe wavelengths were approximated from the raw data (see supporting materials) and this shows that the signal levels are roughly similar. All polarisation combinations clearly show: the rise of signal concomitant with the CTTS excitation (defined as $t = 0$); a subsequent decay over the first picosecond; and a long-time (>3 ps) offset of the signal. The relative amplitudes of the decay and offset vary between the different polarisation combinations and probe wavelengths. For the 1320 nm probe, a significant portion of the signal decays within the first few picoseconds, while for the 800 nm probe the majority of signal remains. At both probe wavelengths, the PS combination has a greater relative long-term offset than PP.

In addition to the amplitude differences, clear differences in the phase dynamics can be seen. Specifically, in the Smix polarisation combination, the phase changes by ~π/2 over the first ps, while the other polarisation combinations show comparatively small phase changes and over longer timescales. The only exception to this is a very fast (sub-100 fs) phase shift near $t = 0$ in the PS polarisation combination with an 800 nm probe.

The amplitudes, $N(t)$, have been fitted to a simple kinetic model:

$$N(t) = g(t) * \{A \exp(-t/\tau) + B\},$$

where A and B are constants, τ is a time constant, and $g(t)$ is a Gaussian instrument response function that has then been convoluted with the exponential decay. The model assumes that the initial signal decays according to first order kinetics into a long-lived product that has a signal level of B, and this subsequently decays on a timescale beyond the measurements. For PP and PS polarisations—where there are only small phase shifts—we fit only the amplitude to this model, while for Smix we additionally fit the phase to the model, but exclude the convolutions with $g(t)$ and any signal before $t = 0$ for this. The lifetimes determined from the fits are given in Table 1.

Although the focus of this work is on the initial solvation dynamics, additional phase-resolved measurements up to 100 ps using 1320 nm probe and the PP polarisation combination were performed and the results are shown in Figure 3. After the initial fast decay of the amplitude, there is a slow decay of the overall signal leaving a constant background at 100 ps. The kinetics have been fitted to a model proposed by Staib and Borgis[25] and this yields two lifetimes of 23±4 ps and 54±13 ps. The context of the fit and these lifetimes will be discussed below.

The intensity of the transient SHG signal is largely determined by the resonance-enhancement of the probe fundamental and/or its SHG. In principle, both the fundamental and SHG can be resonant. Transient absorption spectroscopy of the CTTS reaction from I^- in the bulk (excited at 242 nm) showed that the absorption spectrum rapidly blue-shifts from the IR to the visible on a 0.7 ps timescale (see Figure 1).[4] The final spectrum peaks at ~720 nm and corresponds to the formation of the $[I^0{:}e^-]_{(aq)}$ contact pair. The 0.7 ps lifetime has been

assigned to the reorganisation dynamics of the water molecules to accommodate the new charge distribution. However, these lifetimes are derived from simple fits at a given probe energy, whilst the transient absorption is better described by a continuously shifting absorption spectrum. Therefore, a direct comparison between the lifetimes from our experiment and the transient absorption spectra is mostly qualitative. Additionally, transient fluorescence up-conversion showed that the initially excited CTTS state fluoresces over a broad spectral range spanning 300 – 700 nm (see Figure 1). The broad emission reflects the inhomogeneous environments present as the CTTS is excited and these lead to different dynamics, with the shorter wavelengths showing shorter lifetimes.[26] Because of the very large spectral widths associated with the transient absorption of the solvating $[I^0{:}e^-]_{(aq)}$, and with the emission of the CTTS state, it is nearly impossible to quantitatively disentangle which steps in the SHG are resonant. However, we can use the known bulk energetics, timescales and phase changes to disentangle the dynamics.

On the whole, the amplitude time-constants for the PP and PS data sets are close to, albeit slightly faster, than the 0.7 ps timescale attributed to the equilibration of the solvent surrounding the $[I^0{:}e^-]_{(aq)}$ contact pair in the bulk.[4] The 1320 nm PP and PS data shows that the initial signal is significantly larger relative to the signal after 3 ps compared to the same polarisation combinations at 800 nm. This is consistent with the rapidly blue-shifting absorption spectrum of the $[I{:}e^-]_{(aq)}$ as it solvates, because 1320 nm is more resonant than 800 nm initially (see Figure 4a). Hence, the dynamics observed for PP and PS polarisations are predominantly determined by the probe wavelength (and not its SHG), as shown schematically in Figure 4a. The lack of a phase shift in these polarisation combinations is perhaps surprising, although several excited states may be contributing to these dynamics and predicting how this would be reflected as a phase change is non-trivial.

In contrast to the PP and PS polarisation combinations, the Smix data at both wavelengths shows much faster amplitude kinetics as well as large phase changes on similarly fast timescales. The lifetime for these kinetics and phase changes are comparable to the ~0.2 ps suggested for the decay of the CTTS state to form the non-equilibrated $[I^0{:}e^-]_{(aq)}$ contact pair[4] and is consistent with the timescales reported from the transient fluorescence up-conversion measurements.[26] Therefore, it appears that the Smix polarisation is more sensitive to the CTTS state dynamics rather than the initial solvation of the un-equilibrated $[I^0{:}e^-]_{(aq)}$ as seen for PP and PS. The SHG process from the CTTS state is shown pictorially in Figure 4a. While the solvating contact pair is in its electronic ground states, the CTTS state is an excited electronic state with $I^-_{(aq)}$ as the ground electronic state, as evidenced by the fluorescence spanning 300 – 700 nm from the CTTS state.[26] Thus, the primary resonance that contributes to the kinetics at early times in the Smix polarisation is between the occupied CTTS state and the $I^-_{(aq)}$ ground state. Crucially, only the SHG is resonant. To our knowledge, the CTTS state does not appear in transient absorption spectra with the current probe photon energies. The CTTS then evolves and undergoes a nonadiabatic transition to form the non-equilibrium $[I^0{:}e^-]_{(aq)}$, at which point the SHG signal is once again dominated by the absorption of the solvating $[I^0{:}e^-]_{(aq)}$. The large phase shift observed in Smix is likely related to the rapid decay of the CTTS state, as suggested in Figure 4a. Qualitatively, the initial phases at both probe wavelengths are consistent with the real part of $\chi^{(2)}$ being of different sign at either side of the emission band so that at 400 nm it is closer to $-\pi$, whilst at 660 it is closer to 0. The faster phase dynamics observed at 400 nm than at 660 nm SHG output is also consistent with the transient fluorescence that showed more rapid dynamics at shorter wavelengths.

A most striking point is that only the Smix appears to be sensitive to the CTTS state. Although Smix, PP and PS probe different components of the $\chi^{(2)}$ tensor, the main difference

between Smix and PP or PS is the output polarisation. We have argued that resonance with the second harmonic of the Smix data is mostly responsible for the dynamics observed over the first few 100 fs. Therefore, it appears that the resonant CTTS transition at the interface has a transition dipole moment predominantly aligned along the surface plane, otherwise, both PP and PS would also reveal dynamics associated with the CTTS state. In principle, the PP polarisation combination also contains contributions from the same $\chi^{(2)}$ component probed by Smix. However, we expect this to be relatively small because of the large angle of incidence used in the current experiment such that the response in PP is dominated by components normal to the surface and thus only $[I^0{:}e^-]_{(aq)}$ is probed.

Bradforth and Jungwirth have calculated the electronic structure of the CTTS state of I^- at a water/vacuum interface and concluded that its orbital points towards the solvent (not the vacuum) as it initially occupies a preformed void next to the iodine.[27] The calculated orbital is highly asymmetric. According to their calculations, the orbital is of mixed character: predominantly s- with additional p-character. A radial node exists between the iodine and the extruding diffuse lobe of the CTTS state, which has also been seen in earlier simulations.[28] As shown in Figure 4b, the resonant transition for the SHG in the S-polarised output arises from the transition moment that couples this CTTS back to the I^-(5p) states. For the CTTS state to only be observable by the Smix polarisation therefore requires that there is a preferential alignment of the electron distribution of the CTTS along the surface plane rather than directly into the bulk. Unfortunately, no statistical analysis of the initial localisation of the CTTS state relative to the dividing surface was given in the work of Bradforth and Jungwirth.[27] However, the preferential alignment along the surface plane is consistent with their conclusion that the initial CTTS occupies transient cavities in the first solvation shell around I^-, formed by thermal fluctuations. At the interface, there is a water density gradient normal to the surface. According to simulations of the concentration profile

at the surface, I^- predominantly resides within the region where the water density falls off towards the vapour phase.[15] Hence, the occurrence of preformed cavities is expected to be largest in the plane of the surface next to I^- rather than directly towards the bulk, where the density is higher. This may also account for the slightly faster rates for solvation observed in the present work compared to the bulk. The CTTS state is not expected to extend significantly into the vapour phase as it is bound for a large part by the polarisation of the water around the I^-.[27] Because there is a double layer structure at the electrolyte/air interface[15] that causes a symmetry breakage over ~10 Å, the SHG response may in principle arise from this entire region. However, the CTTS state of I^- in this second layer is effectively as it is in the bulk and is not expected to show the observed asymmetry. Hence, the asymmetric CTTS dynamics probed here reflect the outermost molecular layers of the water/air interface.

The apparent sub-100 fs phase change observed for the 800 nm PS polarisation combination is limited by the time-resolution of the experiment and we can only speculate on its origin. We note that the kinetics show the weakest relative peak at early times implying a lower sensitivity to the non-equilibrated $[I^0{:}e^-]_{(aq)}$. We suggest that perhaps the P output polarisation (PS and PP) is not completely insensitive to the CTTS state dynamics, but is masked by the much larger signals arising from $[I^0{:}e^-]_{(aq)}$. This is not unreasonable because, although on average our results show that the CTTS lies mostly along the surface, there will be a distribution such that some component of the transition moment coupling the CTTS state to the $I^-_{(aq)}$ ground state will lie perpendicular to the surface (as implied in Figure 4b). The 800 nm PS polarisation combination then shows evidence for the CTTS state because of its apparent reduced sensitivity to the non-equilibrated $[I^0{:}e^-]_{(aq)}$ at the early times.

Given our results, deeper insight about surface solvation of the CTTS state and the $[I{:}e^-]_{(aq)}$ may be attained through theoretical modelling of the expected SHG response.

However, this presents a major challenge for theoreticians because of the difficulty in predicting SHG spectra as an infinite sum over all possible pathways involving 2 states, and because of the diffuse nature of the orbitals involved, which include highly polarisable diffuse excited states and the conduction band of water at the interface.[29]

Finally, we have also probed the kinetics of the $[I^0:e^-]_{(aq)}$ contact pair after it has equilibrated (Figure 3). The amplitude shows a slow decay following the initial CTTS and subsequent solvation dynamics. The model proposed by Staib and Borgis[25] has frequently been used to account for the kinetics of the equilibrated $[I^0:e^-]_{(aq)}$, which (ignoring the formation of $[I^0:e^-]_{(aq)}$) involves a competition between geminate recombination to form I^- and the dissociation to form I^0 and $e_{(aq)}^-$ (see Figure 4b). Transient absorption[4,30,31] and photoelectron spectroscopy[12] have been used to monitor these kinetics. Although the photoabsorption wavelength and electron binding energy are insensitive to the difference of these two chemical species, analysis of the kinetics enabled Kloepfer *et al.*[31] to obtain lifetimes of 33 ps for geminate recombination and 70 ps for dissociation of the contact pair. The SHG signal may be expected to be similarly sensitive to both $[I^0:e^-]_{(aq)}$ and $e_{(aq)}^-$ as the absorption spectrum of an interfacial electron has been predicted to be very similar to that of $e_{(aq)}^-$ in the bulk.[32] Therefore, performing the same kinetic analysis of the data in Figure 3 should be appropriate and yields lifetimes of 23±4 ps and 54±13 ps for geminate recombination and dissociation, respectively. This suggests that the kinetics may be slightly faster at the interface. More striking is the small phase shift associated with the kinetics, which occurs over the first ~30 ps. The phase change indicates that, at the surface, $[I^0:e^-]_{(aq)}$ and $e^-_{(aq)}$ can be distinguished. Because the probe wavelength in this experiment was 1320 nm and only the SHG is resonant with transitions of $[I^0:e^-]_{(aq)}$ and $e^-_{(aq)}$ (see Figure 4a), the observed phase shift points to a difference in the absorption spectra of $[I^0:e^-]_{(aq)}$ and $e^-_{(aq)}$ (around 660 nm) at the ambient water/air interface. This is in contrast to the bulk, where no

difference has been noted. The origin for the increased rates of both recombination and dissociation may again be correlated to the lower water density at the interface where the electron resides.

Whether surface electron hydration dynamics are distinct from the bulk has been very topical since the observation of surface binding of hydrated electrons in water clusters[33–35] and thin ice films on metal surfaces[36,37] or metal oxide surfaces.[38] These surface-bound states are distinct from bulk $e^-_{(aq)}$ because most of the electron's distribution is in the vapour phase. The surface-bound state has been observed in a single photoelectron spectroscopy experiment[9] on liquid water microjets, but has not been reproduced in any other experiment. Our experiment shows that, while the initial surface solvation is different, the electron eventually solvates at the interface with physical properties that are very similar to bulk $e^-_{(aq)}$. Hence, this would point to a situation in which the electron does not significantly protrude into the vapour phase. This is consistent with the simulations from Uhlig *et al*. of $e^-_{(aq)}$ at the water/air interface that indicate that the electron solvates in the interfacial water layer and only ~10% of the electron distribution extends into the vapour phase.[39] Nevertheless, the proximity to the vapour phase may have important consequences on its chemical properties as recently implicated in plasma chemistry at the water/air interface.[40] A very recent sum-frequency generation study has also shown a distinctive vibrational spectrum for water interacting with the surface $e^-_{(aq)}$,[41] which resembles the vibrational spectrum of an excess electron in water clusters but not $e^-_{(aq)}$ in the bulk, suggesting the binding site at the interface may be more distinctive than previously thought. These sum-frequency generation experiments are only comparable to the present experiments after ~50 ps where $e^-_{(aq)}$ remains at the surface, but may reflect our suggestion that the $e^-_{(aq)}$ is solvated within a reduced density water environment at the interface, where the hydrogen-bonding network differs to bulk water and may be more closely related to water clusters.

Experimental methods

The time-resolved phase-sensitive lock-in SHG experiment used here has been described in detail elsewhere.[24] The pump beam was derived from an optical parametric amplifier (OPA) pumped by an amplified Ti:sapphire laser system and yielded pulses of 250 nm and ~2.5 μJ pulse^{-1} that were focused at the interface of an aqueous 2M NaI solution. The probe beam was either derived from the same OPA (1320 nm) or the fundamental of the Ti:sapphire amplifier (800 nm), and these were focused onto the same spot on the surface with an angle of incidence of 70° for the probe and 67° for the pump. The pump and probe laser shared the same plane of incidence. The probe produced SHG, a part of which reflected from the surface. Additionally, a fraction of the probe also reflected from the sample surface and propagated collinearly with its SHG. Both the SHG and reflected probe light were then refocused onto a reference surface ([110]-GaAs), where the probe produced a second SHG field which acted as a local oscillator (LO). The LO interfered with the sample SHG that was reflected from the reference surface. The desired polarisation was selected using a Glan-Taylor polariser and the probe fundamental was removed using a prism and filters. The SHG photons were detected using a photomultiplier tube. The phase of the interference between the LO and was controlled by mounting the reference surface on a translation stage: the different phase velocities of the probe fundamental and its SHG in air allowed the phase between the two sources of SHG to be varied by changing the distance between the sample and reference surfaces. To remove the large, constant signal primarily from the LO, we employed a lock-in measurement. In every second laser-shot, a 2 mm SF10 or fused silica window was introduced in the beam path between surface and reference surfaces. The group velocities of the probe fundamental and its SHG were sufficiently different that the SHG from the sample could no longer interfere with the LO. The difference between these two

measurements comprised the lock-in signal and provided excellent stability with respect to drifts in alignment. The absolute phase was determined using quartz as a sample surface. The temporal resolution of the experiment was ~100 fs.

The pump wavelength was chosen to be on the long-wavelength side of the lowest energy bulk I^- CTTS transition since previous SHG[42] and photoelectron spectroscopy[43,44] studies suggested that the transition is red-shifted for I^- at the surface compared to the bulk. We performed experiments using both the S and P polarisations for the pump, but these showed no differences in the results. All the results presented were taken with an S polarised pump beam. Drifts in signal due to changes in surface level of the solution were accounted for by performing periodic background measurements in which the pump was blocked. Over a kinetic scan, these background measurements were fitted to a straight line and this was subtracted from the pump-probe signal. Hence, the kinetic measurements only represent the pump-probe signal arising from the pump (or other products) and the constant background from the electrolyte solution is removed. For some polarisations (primarily PS, but also PP) there is also a "pump-probe signal" that persists between laser pulses due to long-lived products. This was also removed and is discussed in the supporting materials.

Acknowledgements

We are grateful to Colin D. Bain for the many fruitful and insightful discussions. The work has been funded by the Leverhulme Trust and a European Research Council under Starting Grant 306536.

References

(1) Garrett, B. C.; Dixon, D. A.; Camaioni, D. M.; Chipman, D. M.; Johnson, M. A.; Jonah, C. D.; Kimmel, G. A.; Miller, J. H.; Rescigno, T. N.; Rossky, P. J.; et al. Role of Water in Electron-Initiated Processes and Radical Chemistry: Issues and Scientific Advances. *Chem. Rev.* **2005**, *105*, 355–390.

(2) Chen, X.; Bradforth, S. E. The Ultrafast Dynamics of Photodetachment. *Annu. Rev. Phys. Chem.* **2008**, *59*, 203–231.

(3) Long, F. H.; Shi, X.; Lu, H.; Eisenthal, K. B. Electron Photodetachment from Halide Ions in Solution: Excited-State Dynamics in the Polarization Well. *J. Phys. Chem.* **1994**, *98*, 7252–7255.

(4) Iglev, H.; Trifonov, A.; Thaller, A.; Buchvarov, I.; Fiebig, T.; Laubereau, A. Photoionization Dynamics of an Aqueous Iodide Solution: The Temperature Dependence. *Chem. Phys. Lett.* **2005**, *403*, 198–204.

(5) Iglev, H.; Fischer, M. K.; Laubereau, A. Electron Detachment from Anions in Aqueous Solutions Studied by Two- and Three-Pulse Femtosecond Spectroscopy. *Pure Appl. Chem.* **2010**, *82*, 1919–1926.

(6) Kothe, A.; Wilke, M.; Moguilevski, A.; Engel, N.; Winter, B.; Kiyan, I. Y.; Aziz, E. F. Charge Transfer to Solvent Dynamics in Iodide Aqueous Solution Studied at Ionization Threshold. *Phys Chem Chem Phys* **2015**, *17*, 1918–1924.

(7) Pham, V.-T.; Penfold, T. J.; van der Veen, R. M.; Lima, F.; El Nahhas, A.; Johnson, S. L.; Beaud, P.; Abela, R.; Bressler, C.; Tavernelli, I.; et al. Probing the Transition from Hydrophilic to Hydrophobic Solvation with Atomic Scale Resolution. *J. Am. Chem. Soc.* **2011**, *133*, 12740–12748.

(8) Lübcke, A.; Buchner, F.; Heine, N.; Hertel, I. V.; Schultz, T. Time-Resolved Photoelectron Spectroscopy of Solvated Electrons in Aqueous NaI Solution. *Phys. Chem. Chem. Phys.* **2010**, *12*, 14629–34.

(9) Siefermann, K. R.; Liu, Y.; Lugovoy, E.; Link, O.; Faubel, M.; Buck, U.; Winter, B.; Abel, B. Binding Energies, Lifetimes and Implications of Bulk and Interface Solvated Electrons in Water. *Nat. Chem.* **2010**, *2*, 274–279.

(10) Tang, Y.; Shen, H.; Sekiguchi, K.; Kurahashi, N.; Mizuno, T.; Suzuki, Y.-I.; Suzuki, T. Direct Measurement of Vertical Binding Energy of a Hydrated Electron. *Phys. Chem. Chem. Phys.* **2010**, *12*, 3653–3655.

(11) Shreve, A. T.; Yen, T. A.; Neumark, D. M. Photoelectron Spectroscopy of Hydrated Electrons. *Chem. Phys. Lett.* **2010**, *493*, 216–219.

(12) Suzuki, Y.-I.; Shen, H.; Tang, Y.; Kurahashi, N.; Sekiguchi, K.; Mizuno, T.; Suzuki, T. Isotope Effect on Ultrafast Charge-Transfer-to-Solvent Reaction from I^- to Water in Aqueous NaI Solution. *Chem. Sci.* **2011**, *2*, 1094–1102.

(13) Yamamoto, Y.; Suzuki, Y.-I.; Tomasello, G.; Horio, T.; Karashima, S.; Mitríc, R.; Suzuki, T. Time- and Angle-Resolved Photoemission Spectroscopy of Hydrated Electrons Near a Liquid Water Surface. *Phys. Rev. Lett.* **2014**, *112*, 187603.

(14) Sagar, D. M.; Bain, C. D.; Verlet, J. R. R. Hydrated Electrons at the Water/air Interface. *J. Am. Chem. Soc.* **2010**, *132*, 6917–6919.

(15) Jungwirth, P.; Tobias, D. J. Ions at the Air/Water Interface. *J. Phys. Chem. B* **2002**, *106*, 6361–6373.

(16) Chang, R. K.; Ducuing, J.; Bloembergen, N. Relative Phase Measurement between Fundamental and 2nd-Harmonic Light. *Phys. Rev. Lett.* **1965**, *15*, 6–8.

(17) Stolle, R.; Marowsky, G.; Schwarzberg, E.; Berkovic, G. Phase Measurements in Nonlinear Optics. *Appl. Phys. B* **1996**, *63*, 491–498.

(18) Tom, H. W. K.; Heinz, T. F.; Shen, Y. R. 2nd-Harmonic Reflection from Silicon Surfaces and Its Relation to Structural Symmetry. *Phys. Rev. Lett.* **1983**, *51*, 1983–1986.

(19) Veenstra, K. J.; Petukhov, A. V.; de Boer, A. P.; Rasing, T. Phase-Sensitive Detection Technique for Surface Nonlinear Optics. *Phys. Rev. B* **1998**, *58*, R16020–R16023.

(20) Wilson, P. T.; Jiang, Y.; Aktsipetrov, O. A.; Mishina, E. D.; Downer, M. C. Frequency-Domain Interferometric Second-Harmonic Spectroscopy. *Opt. Lett.* **1999**, *24*, 496–498.

(21) McIver, J.; Lee, C.; Torchinsky, D.; Gedik, N. Ultrafast Time- and Phase-Resolved Second Harmonic Generation. In *APS March Meeting*; 2013; p BAPS.2013.MAR.Z23.10.

(22) Nelson, C. A.; Luo, J.; Laghumavarapu, R. B.; Huffaker, D. L.; X.-Y., Z. Time-, Energy-, and Phase-Resolved Second-Harmonic Generation at Semiconductor Interfaces. *J. Phys. Chem. C* **2014**, *118*, 27981–27988.

(23) Wilcox, D. E.; Sykes, M. E.; Niedringhaus, A.; Shtein, M.; Ogilvie, J. P. Heterodyne-Detected and Ultrafast Time-Resolved Second-Harmonic Generation for Sensitive Measurements of Charge Transfer. *Opt. Lett.* **2014**, *39*, 4274–4277.

(24) Nowakowski, P. J.; Woods, D. A.; Bain, C. D.; Verlet, J. R. R. Time-Resolved Phase-Sensitive Second Harmonic Generation Spectroscopy. *J. Chem. Phys.* **2015**, *142*, 84201.

(25) Staib, A.; Borgis, D. Reaction Pathways in the Photodetachment of an Electron from Aqueous Chloride: A Quantum Molecular Dynamics Study. *J. Chem. Phys.* **1996**, *104*, 9027–9039.

(26) Messina, F.; Bräm, O.; Cannizzo, A.; Chergui, M. Real-Time Observation of the Charge Transfer to Solvent Dynamics. *Nat. Commun.* **2013**, *4*, 2119.

(27) Bradforth, S. E.; Jungwirth, P. Excited States of Iodide Anions in Water: A Comparison of the Electronic Structure in Clusters and in Bulk Solution. *J. Phys. Chem. A* **2002**, *106*, 1286–1298.

(28) Sheu, W. S.; Rossky, P. J. Charge-Transfer-to-Solvent Spectra of an Aqueous Halide Revisited via Computer Simulation. *J. Am. Chem. Soc.* **1993**, *115*, 7729–7735.

(29) Jacobson, L. D.; Herbert, J. M. Polarization-Bound Quasi-Continuum States Are Responsible for The "blue Tail" in the Optical Absorption Spectrum of the Aqueous Electron. *J. Am. Chem. Soc.* **2010**, *132*, 10000–10002.

(30) Kloepfer, J. A.; Vilchiz, V. H.; Lenchenkov, V. A.; Bradforth, S. E. Femtosecond Dynamics of Photodetachment of the Iodide Anion in Solution : Resonant Excitation into the Charge-Transfer-to-Solvent State. *Chem. Phys. Lett.* **1998**, *298*, 120–128.

(31) Kloepfer, J. A.; Vilchiz, V. H.; Lenchenkov, V. A.; Germaine, A. C.; Bradforth, S. E. The Ejection Distribution of Solvated Electrons Generated by the One-Photon Photodetachment of Aqueous I^- and Two-Photon Ionization of the Solvent. *J. Chem. Phys.* **2000**, *113*, 6288–6306.

(32) Uhlig, F.; Herbert, J. M.; Coons, M. P.; Jungwirth, P. Optical Spectroscopy of the Bulk and Interfacial Hydrated Electron from Ab Initio Calculations. *J. Phys. Chem. A* **2014**, *118*, 7507–7515.

(33) Verlet, J. R. R.; Bragg, A. E.; Kammrath, A.; Cheshnovsky, O.; Neumark, D. M. Observation of Large Water-Cluster Anions with Surface-Bound Excess Electrons. *Science* **2005**, *307*, 93–96.

(34) Coe, J. V.; Arnold, S. T.; Eaton, J. G.; Lee, G. H.; Bowen, K. H. Photoelectron Spectra of Hydrated Electron Clusters: Fitting Line Shapes and Grouping Isomers. *J. Chem. Phys.* **2006**, *125*, 14315.

(35) Ma, L.; Majer, K.; Chirot, F.; von Issendorff, B. Low Temperature Photoelectron Spectra of Water Cluster Anions. *J. Chem. Phys.* **2009**, *131*, 144303.

(36) Bovensiepen, U.; Gahl, C.; Stähler, J.; Bockstedte, M.; Meyer, M.; Baletto, F.; Scandolo, S.; Zhu, X. Y.; Rubio, A.; Wolf, M. A Dynamic Landscape from Femtoseconds to Minutes for Excess Electrons at Ice-Metal Interfaces. *J. Phys. Chem. C* **2009**, *113*, 979–988.

(37) Stähler, J.; Deinert, J.-C.; Wegkamp, D.; Hagen, S.; Wolf, M. Real-Time Measurement of the Vertical Binding Energy during the Birth of a Solvated Electron. *J. Am. Chem. Soc.* **2015**, *137*, 3520–3524.

(38) Zhao, J.; Li, B.; Onda, K.; Feng, M.; Petek, H. Solvated Electrons on Metal Oxide Surfaces. *Chem. Rev.* **2006**, *106*, 4402–4427.

(39) Uhlig, F.; Marsalek, O.; Jungwirth, P. Unraveling the Complex Nature of the Hydrated Electron. *J. Phys. Chem. Lett.* **2012**, *3*, 3071–3075.

(40) Rumbach, P.; Bartels, D. M.; Sankaran, R. M.; Go, D. B. The Solvation of Electrons by an Atmospheric-Pressure Plasma. *Nat. Commun.* **2015**, *6*, 7248.

(41) Matsuzaki, K.; Kusaka, R.; Nihonyanagi, S.; Yamaguchi, S.; Nagata, T.; Tahara, T. Partially Hydrated Electrons at the Air/Water Interface Observed by UV-Excited Time-Resolved Heterodyne-Detected Vibrational Sum Frequency Generation Spectroscopy. *J. Am. Chem. Soc.* **2016**, *138*, 7551–7557.

(42) Petersen, P. B.; Johnson, J. C.; Knutsen, K. P.; Saykally, R. J. Direct Experimental Validation of the Jones–Ray Effect. *Chem. Phys. Lett.* **2004**, *397*, 46–50.

(43) Hiranuma, Y.; Kaniwa, K.; Shoji, M.; Mafuné, F. Solvation Structures of Iodide on and below a Surface of Aqueous Solution Studied by Photodetachment Spectroscopy. *J. Phys. Chem. A* **2011**, *115*, 8493–8497.

(44) Shoji, M.; Kaniwa, K.; Hiranuma, Y.; Maselli, O.; Mafuné, F. Solvation Structure of I^- and Na^+ on the Surface of NaI Aqueous Solution Studied by Photodetachment Spectroscopy in Combination with Mass Spectrometry. *J. Phys. Chem. A* **2011**, *115*, 2148–2154.

Polarisation	τ (1320 nm) / ps	τ (800 nm) / ps
PP	0.50 ±0.02	0.48 ±0.03
PS	0.67 ±0.06	0.7 ±0.2
Smix (amplitude)	0.16 ±0.01	0.34 ±0.02
Smix (phase)	0.46 ±0.04	< 0.4

Table 1. Fitted time constants. The uncertainties are obtained from the fitting procedure although we believe they are an underestimate of the real uncertainty in the time constants. For Smix at 800 nm we present an estimate rather than a fit to the phase kinetics.

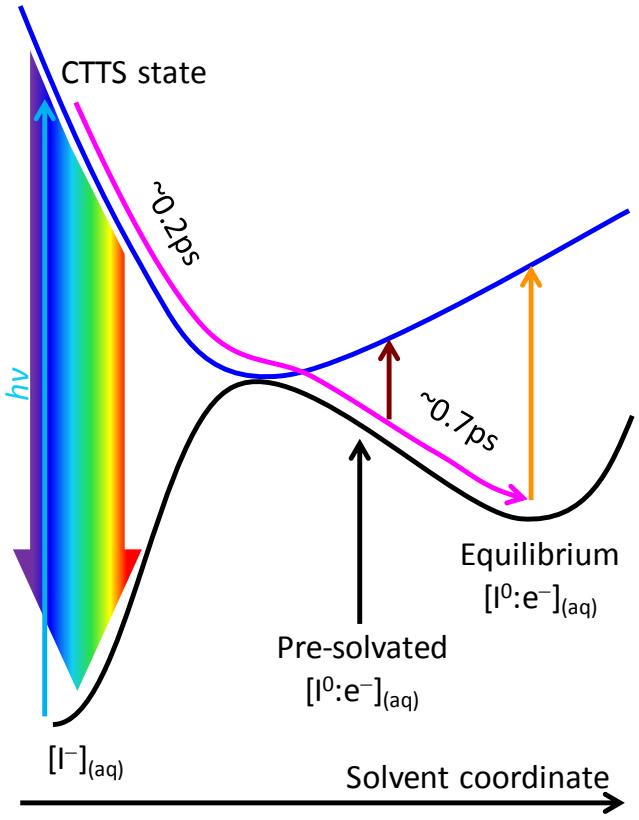

Figure 1. Schematic of CTTS reaction dynamics in the bulk. Photoexcitation of $[I^-]_{(aq)}$ in the UV produces the CTTS state. This then undergoes a nonadiabatic transition to for a pre-solved $[I^0{:}e^-]_{(aq)}$ contact pair which occurs on a roughly 200 fs timescale. Once on the ground state, the water solvates the non-equilibrium contact pair on a roughly 700 fs timescale to generate $[I^0{:}e^-]_{(aq)}$. The CTTS state has previously been characterised by fluorescence while the solvation of $[I^0{:}e^-]_{(aq)}$ by transient absorption and photoelectron spectroscopy.

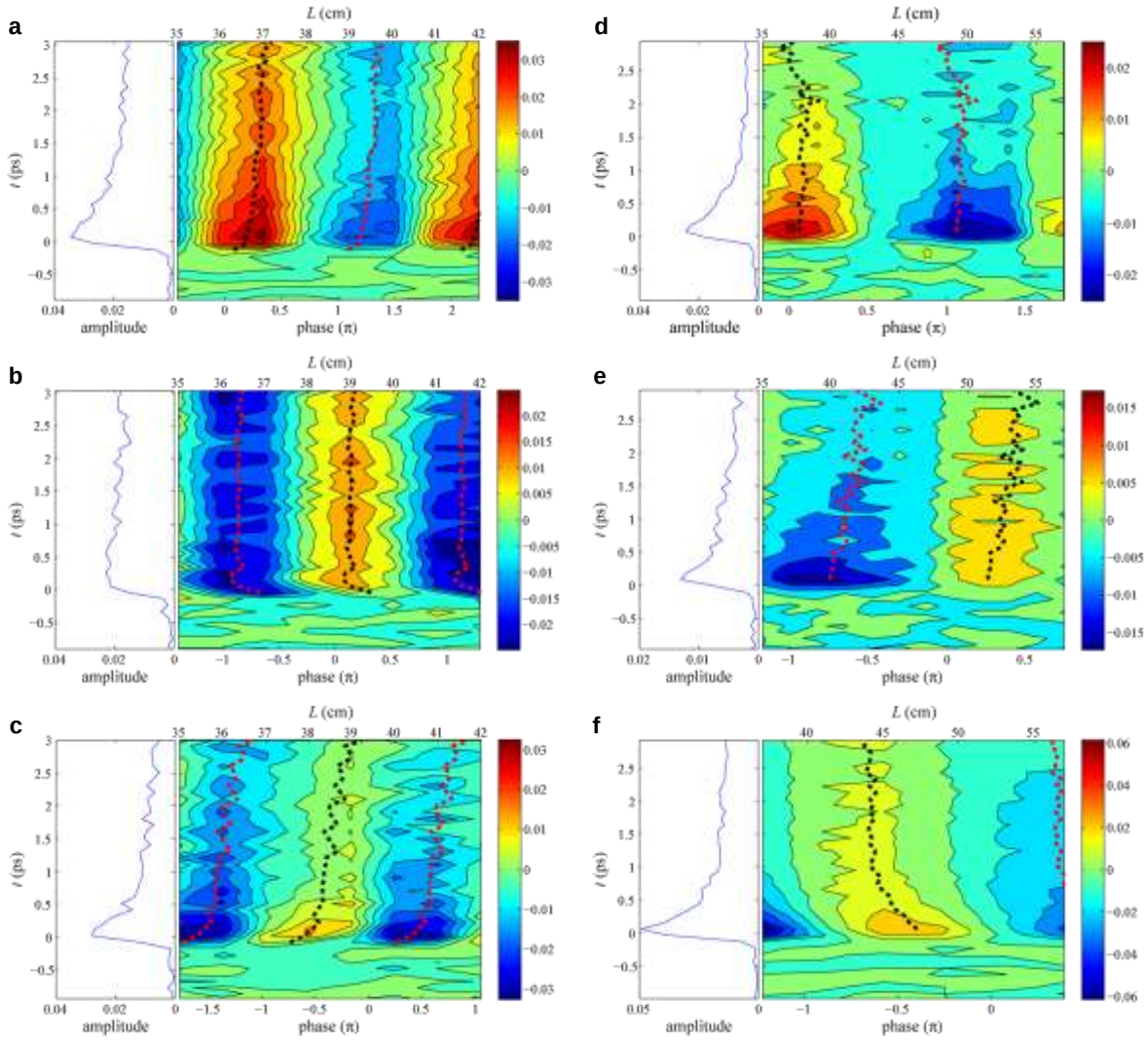

Figure 2. Kinetics of the CTTS solvation dynamics at a variety of polarisations and wavelengths. Panels **a** - **c** show dynamics with an 800 nm probe (400 nm SHG) and **d** – **f** with a 1320 nm probe (660 nm SHG). Different polarisation combinations are shown in rows: PP in **a** and **d**, PS in **b** and **e**, and Smix in **c** and **f**. The contour plot shows the signal from the lock-in measurement as a function of stage position (*L* (cm), top axis), with the corresponding absolute phase on the bottom axis (black dashed line; red dashed line is phase ±π). The left-hand side of each plot shows the amplitude of the signal. The vertical axis corresponds to the delay between the CTTS excitation pulse and the probe.

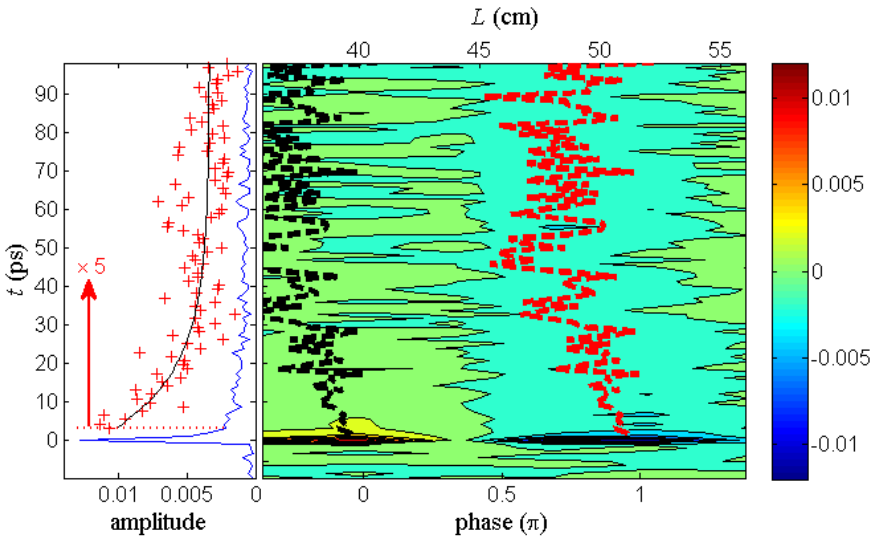

Figure 3. Kinetics over the first 100 ps following CTTS excitation**.** Plot shows the same information as Figure 1 but over an extended timescale. The dynamics were probed with PP polarisation combination and at 1320 nm (660 nm SHG). The amplitude has been scaled by a factor of 5 to highlight the decay after the initial fast kinetics. The solid black line through this is the fit to the kinetics.

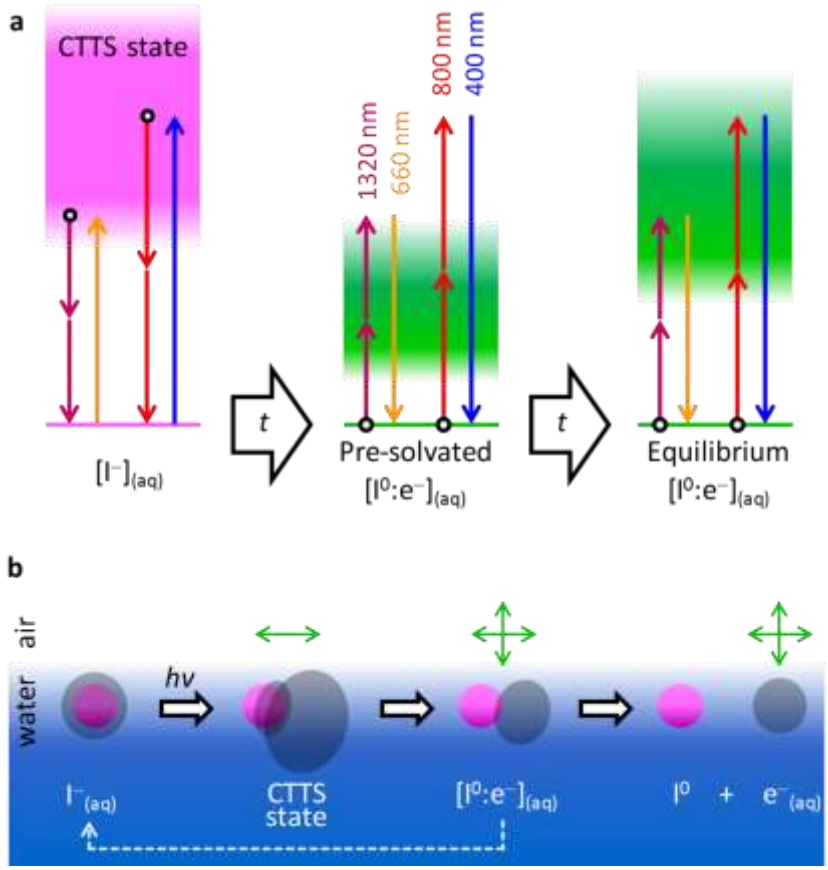

Figure 4. Schematic of transitions leading the SHG and the surface CTTS reaction. Panel **a** shows that the SHG response of the pre-solvated $[I^0{:}e^-]_{(aq)}$ contact pair is initially dominated by "absorption" transitions with the fundamental at 1320 nm and to a lesser extent 800 nm. The initial CTTS state response involves primarily "emission" transitions from the CTTS state to $I^-_{(aq)}$ that are resonant with the second harmonic of the probes. Equilibrated $[I^0{:}e^-]_{(aq)}$ is probed by transitions as shown. Panel **b** shows that photo-excitation produces a CTTS state that is predominantly aligned in the plane of the interface so that transitions that are S polarised (double arrow) predominantly probe this CTTS state. In contrast, $[I^0{:}e^-]_{(aq)}$ can be probed by any polarisation. The contact pair can dissociate to form $e^-_{(aq)}$ that can be probed by any polarisation or recombine to yield I^- (dashed arrow).